Article

Thermal Expansion and Polymorphism of Slawsonite SrAl$_2$Si$_2$O$_8$

Liudmila Gorelova [1,*] , Oleg Vereshchagin [1] and Anatoly Kasatkin [2]

1   Institute of Earth Sciences, Saint Petersburg State University, University Embankment 7/9, 199034 St. Petersburg, Russia; o.vereshchagin@spbu.ru
2   Fersman Mineralogical Museum of the Russian Academy of Sciences, Leninskiy Prospect. 18, 119071 Moscow, Russia; kasatkin@inbox.ru
*   Correspondence: l.gorelova@spbu.ru

Abstract: Slawsonite's (SrAl$_2$Si$_2$O$_8$) structure evolutions depending on temperature (27–1000 °C) have been studied by in situ single-crystal X-ray diffraction. The SrO$_7$ polyhedron expands regularly with the temperature increase. Silicon and aluminum cations are ordered in tetrahedral sites of the studied slawsonite; no significant changes in their distribution as temperature increases were observed. Slawsonite demonstrates a relatively high volume thermal expansion ($\alpha_V = 23 \times 10^{-6}$ °C^{-1}) with high anisotropy, typical for framework feldspar-related minerals and synthetic compounds. It was found that, contrary to previously published data, the crystal structure of slawsonite is stable in the studied temperature range and no phase transitions occur up to 1000 °C. The role of Ca and Ba substitution for Sr and Al/Si ordering on polymorphism of natural MAl$_2$Si$_2$O$_8$ (M = Ca, Sr, Ba) is herein discussed.

Keywords: slawsonite; feldspar; crystal structure; thermal expansion; high temperature; single-crystal X-ray diffraction

1. Introduction

The alkaline earth aluminosilicates with the general formula MAl$_2$Si$_2$O$_8$ (M = Ca, Sr, Ba) are very important both for geology and material sciences. On the one hand, they relate to the feldspars, which are the most common minerals in the Earth's crust, on the other hand, they are applied as ceramic components [1–3], phosphorous (e.g., [4–9]), refractories material [10] and matrix for radioactive wastes [11–13]. According to the Commission on New Minerals, Nomenclature and Classification (CNMNC) of the International Mineralogical Association (IMA), only one mineral with the composition of SrAl$_2$Si$_2$O$_8$, i.e., slawsonite, is known up to date. Whereas its Ca and Ba analogs exist in nature in four (namely, anorthite, dmisteinbergite, svyatoslavite, and stoefflerite) and three (celsian, hexacelsian, and paracelsian) polymorphic modifications with different topology, respectively [14].

As was mentioned above, slawsonite belongs to the feldspar group of minerals. According to a recent review on feldspars [14], all the feldspar-related crystal structures are divided into three groups: tetrahedral structures, octahedral structures, and structures with mixed coordination numbers. Wherein the first group is the most widespread in nature and the last one has not been found in nature at all. In turn, the tetrahedral structures are subdivided into four groups, based on the structural topology, i.e., feldspar, paracelsian, svyatoslavite (all three correspond to three-dimensional frameworks), and dmisteinbergite (layered). According to the classification [14], slawsonite together with paracelsian (BaAl$_2$Si$_2$O$_8$), danburite- (MB$_2$Si$_2$O$_8$, M = Ca, Sr, Ba) and hurlbutite-group minerals (MBe$_2$P$_2$O$_8$, M = Ca, Sr) belong to the minerals with the paracelsian topology.

Slawsonite is quite a rare mineral, which has been found only in several localities and is usually associated with metasomatic reactions at low temperatures and low-pressure metamorphism [15]. As a mineral, slawsonite has been first described in Martin Bridge

formation, Oregon, the USA by Griffen et al. in 1977 [16], whereas its synthetic analog had already been known [17]. Moreover, according to the Inorganic Crystal Structure Database (ICSD) the synthetic compound with the general formula $SrAl_2Si_2O_8$ is known at least in four other polymorphic modifications: $I2/c$ [18–21], $P–3c$ [22], $P6_3/mcm$ [22,23] and $Pm–3m$ [24]. It is interesting to note, that according to Bahat [25] the hexagonal modification of $SrAl_2Si_2O_8$ (as well as $CaAl_2Si_2O_8$) does not have any fields of stability under ambient pressure, whereas hexagonal $BaAl_2Si_2O_8$ can exist under ambient conditions, which is probably associated with the increase of the ionic size of the M^{2+} (M = Ca, Sr, Ba) cation.

Due to the high geological importance and wide industrial implications, many minerals with the feldspar topology were studied in detail both under ambient and extreme conditions (high- and low temperatures and high pressures). Though feldspar minerals with the paracelsian topology are not very widespread in nature, almost all of them (except strontiohurlbutite) have been recently studied under high-pressure conditions [26–30], whereas only danburite-group minerals have been studied in detail under temperature increase up to the present time [31,32].

To date, it is known, that generally, the polymorphism of $SrAl_2Si_2O_8$ is similar to that of $BaAl_2Si_2O_8$. However, as most of the published results have been obtained by transmission electron microscopy and powder X-ray diffraction, many inconsistencies occur. It is thought that slawsonite has a displacive phase transition at 320 °C from triclinic to monoclinic phase [33,34]. According to [35,36] at 500 or 600 °C slawsonite transforms into another monoclinic phase, namely Sr-celsian (i.e., compound with the feldspar topology), which melts at 1650 °C. Nevertheless, this phase transition was not mentioned by Tagai et al. [33], who performed differential thermal analysis (DTA) up to 1000 °C. Three hexagonal (or pseudohexagonal) $SrAl_2Si_2O_8$ polymorphs ($P6/mmm$, $P6_3/mcm$, and $Immm$), similar to hexacelsians ($BaAl_2Si_2O_8$) [37] can be obtained by quenching melt. According to Toepel-Schadt et al. [36], two hexagonal phases coexist at room temperature and the transition to orthorhombic phase occurs at about 600 °C [38].

The present study aims to investigate the high-temperature behavior of slawsonite using in situ single-crystal X-ray diffraction data at a temperature range of 27–1000 °C in order to clarify whether there are phase transitions and compare the obtained data with the data on other isotypic minerals.

2. Materials and Methods

The natural sample of slawsonite, $SrAl_2Si_2O_8$, originating from the Rendai, Kochi Prefecture, Shikoku Island, Japan, was obtained from the private systematic collection of AK. The chemical composition of this sample has stochiometry close to ideal ($Sr_{0.94}Ba_{0.03}Al_{1.97}Si_{2.04}O_8$; [29]).

Thermal behavior of slawsonite under heating in the air was studied in situ by high-temperature single-crystal X-ray diffraction (SCXRD) using a XtaLAB Synergy-S diffractometer (Rigaku Oxford Diffraction, Japan) operated with monochromated MoKα radiation (λ[MoKα] = 0.71073 Å) at 50 kV and 40 mA and equipped with an HyPix-6000HE detector with a unique high-temperature FMB Oxford system. The sample heating is done using a gas blower (Figure 1a) up to 1000 ($\pm$1) °C, which consists of a hot air generator controlled by a Eurotherm regulator and gas flow controller. The temperature stability is about $\pm$0.5 °C at the temperature above 250 °C, the heating rate is about 10 °C/min for the temperatures below 400 °C and 5 °C/min from 400 to 1000 °C. Before the experiments, the accuracy of this device has been verified using a single crystal of quartz, which has an $\alpha\leftrightarrow\beta$ transformation at 573 °C [39]. The temperature determination error is $\pm$10 °C. After heating, the crystal was kept at each temperature for about 10 min and after that, the SCXRD data were collected (that took about 20 min at each temperature point). For this experiment, the single crystal with the approximate size of 30 µm × 30 µm × 10 µm was mounted on the glass fiber, which was placed into the quartz capillary (Figure 1b) 300 µm in outer diameter and 10 µm of wall thickness, produced by Hampton Research (USA). Diffraction data were collected at different temperatures without changing the orientation of the crystal in the range of 27 to 1000 °C with a temperature step of 100 °C. The frame

width was 1.0° in ω and φ, the exposure of 3 s per frame. The data were integrated and corrected for background, Lorentz, and polarization effects. An empirical absorption correction based on the spherical harmonics implemented in the SCALE3 ABSPACK algorithm was applied in the CrysAlisPro program [40]. The unit-cell parameters were refined using the least-square techniques. The SHELXL program package [41] was used for all structural calculations. At temperatures below 300 °C, the crystal structures of slawsonite were refined in both possible space groups ($P2_1/c$ and $P–1$) (see below for details). The structure models of natural slawsonite by Griffen et al. [16] ($P2_1/c$) and Tagai et al. [33] ($P–1$) were used as starting models for structure refinements. The crystal structures were refined at 11 temperature points (Tables 1 and 2), including room temperature after heating. Anisotropic displacement parameters were refined for all atoms.
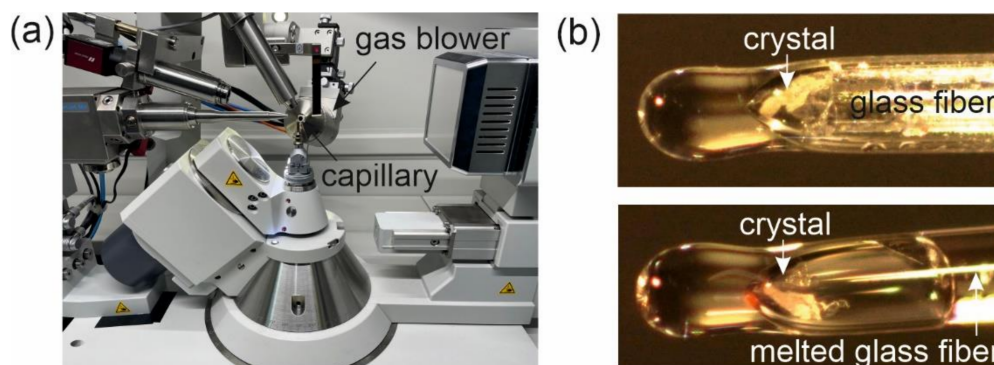
Figure 1. Equipment used for the in situ high-temperature single-crystal study: (**a**) the gas blower (FMB Oxford) inside the XtaLAB Synergy-S diffractometer (Rigaku Oxford Diffraction); (**b**) slawsonite crystal in the quartz capillary at 27 (**above**) and 1000 °C (**below**).

The temperature dependencies of the unit-cell parameters were described by quadratic and linear (for comparison with other minerals) polynomial functions in the whole temperature range (see below for more details).

Based on these data, the thermal expansion coefficients (α_a (°C^{-1}) = $(1/a)(\mathrm{d}a/\mathrm{d}T)$) were determined using the TTT program package [42,43]. This program package has also been used for the thermal-expansion parameter tensor visualization.

3. Results and Discussion

3.1. Polymorphism of Natural $SrAl_2Si_2O_8$ in a Temperature Range 27–1000 °C

Generally, the crystal structure of slawsonite is based on a three-dimensional tetrahedral framework that contains four- and eight-membered rings of SiO_4 and AlO_4 tetrahedra [16], framework channels are occupied by Sr atoms (Figure 2). However, if this crystal structure is compared with other feldspar-related minerals, it could be described as consisting of the crankshaft chains of tetrahedral (Figure 3a), formed by the successive polymerization of four-membered rings [44].

The temperature dependencies for the unit cell parameters, obtained during our SCXRD experiment, and the evolution of normalized unit cell parameters are shown in Figures 4 and 5, respectively. In the whole temperature range (up to 1000 °C) the crystal structure of slawsonite undergoes a continuous expansion of the unit-cell parameters. At the first glance, the changes of the unit-cell parameters are not linear and should be divided into three parts (from 27 to 200, from 300 to 700, and from 800 to 1000 °C), i.e., demonstrate two possible phase transformations (at about 300 and 700 °C). According to the SCXRD and DTA data by Tagai et al. [33] a phase transition should occur at 320 °C with the symmetry increasing from $P–1$ to $P2_1/c$. The second phase transition has been previously mentioned at 500 or 600 °C [34,35] but has not been confirmed by Tagai et al. [33]. According to SCXRD data by Tagai et al. [33], collected below 320 °C, there are some weak but sharp reflections, which are excluded by the space group $P2_1/c$ and as a consequence, the real structure of slawsonite under ambient conditions has to be triclinic. Our SCXRD data at all temperature

points contain about 150 very weak reflections (<3σ) and only 1–5 relatively low reflections (>3σ) (see supplementary crystallographic information data files). Our attempts to refine the crystal structure of slawsonite at temperatures below 220 °C in the triclinic symmetry did not demonstrate any improvements over the refinements in the monoclinic symmetry (Tables 1–4): *R*-factors were almost the same regardless of symmetry and even better for the $P2_1/c$ space group. Besides, the bond length errors are also the same for both space groups. According to both Tagai et al. [33] and our data (Tables 1–4), there is Si-Al order in tetrahedra. Moreover, our data shows that crystal structure is fully ordered in the whole temperature range (<Si–O> = 1.616–1.622, <Al–O> = 1.743–1.749 Å under ambient conditions), i.e., no disordering occur in tetrahedra ((Si–O) = 1.64, (Al–O) = 1.77 Å; [45]). Thus, the only opportunity for $P2_1/c \rightarrow P-1$ transition could be Sr/Ba ordering. As there are no strong crystal-chemical reasons to decrease the symmetry, we suppose the absence of the phase transition at 300 °C. A similar situation is with the second inflection of the unit cell parameters between 700 and 800 °C: according to the SCXRD data, the crystal structure does not undergo any phase transformation. The similar non-linear behavior of the unit cell parameters without any phase transformations has been previously observed for slawsonite [29] and some other isotypic minerals (danburite-group minerals $MB_2Si_2O_8$ (M = Ca, Sr, Ba) [26,28], paracelsian $BaAl_2Si_2O_8$ [27], hurlbutite $CaBe_2P_2O_8$ [30]) under high-pressure conditions. As a consequence, for further discussion, we will use the crystal structure of slawsonite refined in the monoclinic $P2_1/c$ space group at all temperatures.
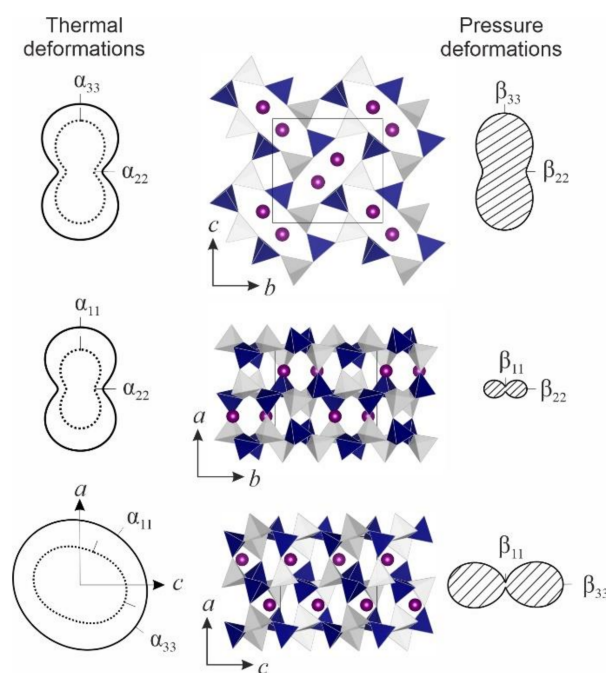
Figure 2. Crystal structure of slawsonite with the section of thermal expansion and pressure compression coefficients. AlO_4 and SiO_4 tetrahedra are given in grey and blue, respectively. Sr atoms are presented as purple spheres. Thermal expansion and pressure compression coefficients along the principal axes of deformations tensors are labeled by α and β, respectively.

Though the crystals studied by Tagai et al. [33] and by us are from the same locality (Kochi Prefecture, Shikoku Island, Japan) and the chemical composition is very close (Sr/Ba ≈ 0.95/0.05), the different high-temperature behavior could be explained by the blockiness of the crystals: some domains could indeed have triclinic crystal structures, but the average crystal structure is better described by the monoclinic ($P2_1/c$) space group in the whole temperature range. The other option could be that two polymorphs are present in the same deposit: low-slawsonite (Sp. gr. $P-1$, described by Tagai et al. [33]) and high-slawsonite (Sp. gr. $P2_1/c$, described by us). Low-slawsonite could be a result of Sr/Ba ordering at the 7-coordinated site or there is slightly higher Ba content, which resulted

in phase transition ([VII]Sr–O 2.61, [VII]Ba–O 2.78 Å; [43]): compare 2.651 Å [33] and 2.644 Å (Tables 3 and 4).
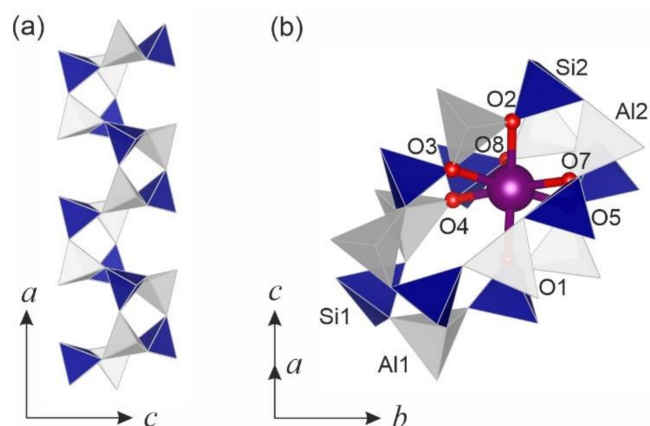
Figure 3. Fragments of the crystal structure of slawsonite: double crankshafts running along with the *a*-axis (**a**); SrO$_7$ polyhedron in ball-and-stick representation in the cavity of eight-membered rings of *T*O$_4$ (*T* = Si, Al) tetrahedra (**b**). AlO$_4$ and SiO$_4$ tetrahedra are given in grey and blue, respectively. Purple and red balls indicate Sr and O atoms, respectively.
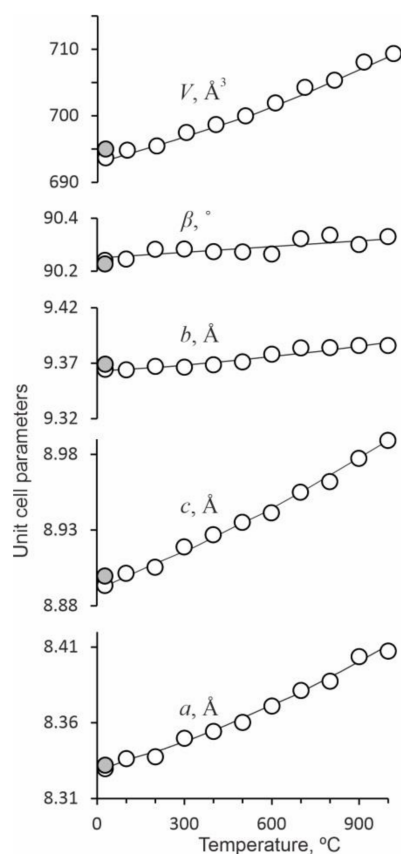
Figure 4. Unit-cell parameters (*a*, *b*, *c*, *β*, *V*) of slawsonite at different temperatures. The white symbols show the unit cell parameters on heating, the grey one – at room temperature after heating. The errors are smaller than the symbols.
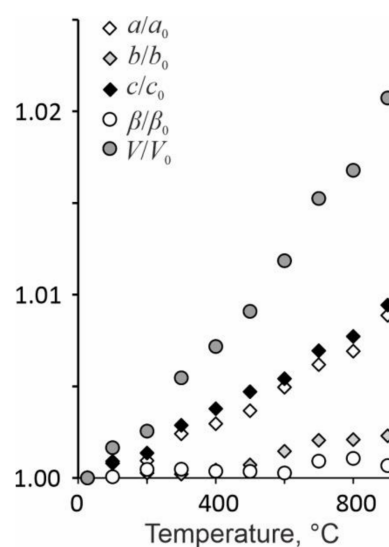
Figure 5. Evolution of normalized unit-cell parameters (a/a_0, b/b_0, c/c_0, β/β_0; V/V_0, where a, b, c, β, V are the unit cell parameters at each temperature and a_0, b_0, c_0, β_0, V_0 are the unit cell parameters at room temperature) of slawsonite.

Besides the suspected displacive phase transition [33], a reconstructive transformation into Sr-feldspar (namely in the crystal structure with the feldspar topology, isostructural to celsian) at the temperature of about 500–600 °C was also proposed [35,36]. Our data demonstrate the absence of both phase transitions. However, the chemical composition of the samples transformed to the 'Sr-feldspar' form has not been studied. Thus, it can be assumed that the presence of even small Sr to Ba substitution can play an important role in the stabilization process of the slawsonite form of the crystal structure and Sr/Ba/□ (vacancy) ratio could result in unexpected phase transitions (e.g., [46]).

Previously, partial replacement of Sr by Ca in slawsonite has been reported from metamorphosed limestones [16,46], and veinlets in metamorphosed xenoliths [47,48]. Barium for strontium substitution was detected in slawsonite from xenolith in an ultramafic rock [33,47]. Both calcium and barium were found in slawsonites from a picrite sill [34] and an analcime syenite ("teschenite"; [15]). As slawsonites always occur as small grains, there are limited data on the crystallography of these (Sr, Ba, Ca)$Al_2Si_2O_8$ phases, and careful structural analysis is needed.

Table 1. Crystallographic data and refinement parameters for slawsonite $SrAl_2Si_2O_8$ at different temperatures in the $P2_1/c$ space group.

Temperature, °C	27	100	200	300	400	500	600	700	800	900	1000	27
Temperature Point	T00	T01	T02	T03	T04	T05	T06	T07	T08	T09	T10	T11
Space group						$P2_1/c$						
a, Å	8.3298(6)	8.3364(6)	8.3376(6)	8.3498(7)	8.3544(7)	8.3603(8)	8.3710(9)	8.381(1)	8.387(1)	8.404(1)	8.407(1)	8.3320(7)
b, Å	9.3645(7)	9.3641(7)	9.3670(7)	9.3664(7)	9.3685(8)	9.3711(9)	9.3781(9)	9.3837(7)	9.384(1)	9.3860(9)	9.3859(9)	9.3677(6)
c, Å	8.8934(8)	8.9014(7)	8.9054(8)	8.9189(8)	8.9269(9)	8.9352(9)	8.942(1)	8.9551(7)	8.962(1)	8.9773(9)	8.989(1)	8.8887(7)
β, °	90.242(8)	90.246(8)	90.283(9)	90.285(9)	90.27(1)	90.27(1)	90.26(1)	90.323(9)	90.34(1)	90.30(1)	90.33(1)	90.229(7)
Volume, Å³	693.7(1)	694.86(9)	695.5(1)	697.5(1)	698.7(1)	700.0(1)	701.9(1)	704.3(1)	705.4(2)	708.1(1)	709.4(1)	694.55(9)
Z							4					
Data collection												
Wavelength, Å							0.71073					
Max. θ°	29.343	29.310	29.304	29.458	29.442	29.421	29.385	29.173	29.144	29.093	29.226	29.334
Index ranges	$-11 \leq h \leq 11$ $-8 \leq k \leq 12$ $-11 \leq l \leq 9$	$-11 \leq h \leq 11$ $-8 \leq k \leq 12$ $-11 \leq l \leq 9$	$-11 \leq h \leq 11$ $-8 \leq k \leq 12$ $-11 \leq l \leq 9$	$-11 \leq h \leq 11$ $-8 \leq k \leq 12$ $11 \leq l \leq 9$	$-11 \leq h \leq 11$ $-8 \leq k \leq 12$ $-11 \leq l \leq 9$	$-11 \leq h \leq 11$ $-8 \leq k \leq 12$ $-11 \leq l \leq 9$	$-11 \leq h \leq 11$ $-8 \leq k \leq 12$ $-11 \leq l \leq 9$	$-11 \leq h \leq 10$ $-7 \leq k \leq 12$ $-11 \leq l \leq 11$	$-10 \leq h \leq 11$ $-7 \leq k \leq 12$ $-11 \leq l \leq 11$	$-11 \leq h \leq 9$ $-7 \leq k \leq 12$ $-11 \leq l \leq 11$	$-11 \leq h \leq 9$ $-7 \leq k \leq 12$ $-12 \leq l \leq 11$	$-11 \leq h \leq 9$ $-8 \leq k \leq 12$ $-12 \leq l \leq 11$
No.meas.refl.	4772	4736	4806	4773	4789	4814	4830	4876	4796	4559	4263	4628
No.uniq.refl.	1529	1522	1542	1538	1539	1543	1554	1590	1576	1567	1578	1557
No. obs.refl($I > 2\sigma(I)$)	1249	1207	1203	1164	1132	1138	1076	1081	958	979	831	1191
Refinement of the structure												
No.of variables							118					
R_{int}	0.0364	0.0382	0.0413	0.0500	0.0443	0.0467	0.0486	0.0481	0.0656	0.0520	0.0670	0.0453
R_1, all data	0.0528	0.0526	0.0577	0.0648	0.0641	0.0712	0.0776	0.0866	0.1032	0.1077	0.1255	0.0662
R_1, $I > 2\sigma(I)$	0.0352	0.0343	0.0371	0.0390	0.0367	0.0408	0.0404	0.0448	0.0500	0.0507	0.0476	0.0400
wR_2, all data	0.0774	0.0731	0.0808	0.0856	0.0808	0.0873	0.0929	0.0944	0.1261	0.1020	0.1117	0.0840
wR_2, $I > 2\sigma(I)$	0.0716	0.0676	0.0733	0.0779	0.0732	0.0788	0.0813	0.0821	0.1069	0.0865	0.0890	0.0761
GooF	1.041	1.036	1.056	1.029	0.984	1.027	0.988	1.038	0.988	1.032	0.932	1.035

Table 2. Crystallographic data and refinement parameters for slawsonite $SrAl_2Si_2O_8$ at different temperatures in the $P–1$ space group.

Temperature, °C	27	100	200
Temperature Point	**T00**	**T01**	**T02**
Space group		$P–1$	
a, Å	8.3243(8)	8.3289(8)	8.3326(9)
b, Å	8.8940(8)	8.9033(8)	8.9056(9)
c, Å	9.3705(9)	9.3706(9)	9.3730(9)
α, °	90.172(8)	90.155(8)	90.129(8)
β, °	90.086(8)	90.086(8)	90.053(8)
γ, °	90.270(8)	90.263(8)	90.306(8)
Volume, Å^3	693.75(11)	694.86(11)	695.53(12)
Z		4	
Data collection			
Wavelength, Å		0.71073	
Max. θ°	29.352	29.339	29.312
Index ranges	$-11 \leq h \leq 11$ $-9 \leq k \leq 11$ $-12 \leq l \leq 8$	$-11 \leq h \leq 11$ $-9 \leq k \leq 11$ $-12 \leq l \leq 8$	$-11 \leq h \leq 1$ $1-9 \leq k \leq 11$ $-12 \leq l \leq 8$
No.meas.refl.	4976	4918	4982
No.uniq.refl.	2693	2679	2705
No. obs.refl($I > 2\sigma(I)$)	2045	2005	1985
Refinement of the structure			
No.of variables	235	235	230
R_{int}	0.0372	0.0430	0.0424
R_1, all data	0.0671	0.0716	0.0777
R_1, $I > 2\sigma(I)$	0.0375	0.0401	0.0430
wR_2, all data	0.0848	0.0913	0.0999
wR_2, $I > 2\sigma(I)$	0.0772	0.0826	0.0884
GooF	1.003	1.024	1.025

Table 3. Bond distances and polyhedral parameters in slawsonite $SrAl_2Si_2O_8$ at different temperatures in the $P2_1/c$ space group.

Temperature, °C	27	100	200	300	400	500	600	700	800	900	1000	27
Temperature Point	T00	T01	T02	T03	T04	T05	T06	T07	T08	T09	T10	T11
SiO₄ tetrahedra												
Si1–O1	1.622(3)	1.619(3)	1.621(4)	1.622(4)	1.623(4)	1.622(4)	1.620(4)	1.617(5)	1.607(7)	1.613(6)	1.612(6)	1.615(4)
Si1–O4	1.624(3)	1.621(3)	1.621(4)	1.620(4)	1.615(4)	1.620(4)	1.618(4)	1.620(5)	1.619(6)	1.616(5)	1.621(6)	1.626(4)
Si1–O5	1.612(3)	1.614(3)	1.619(3)	1.615(4)	1.612(4)	1.610(4)	1.610(4)	1.613(4)	1.616(5)	1.612(4)	1.612(5)	1.615(4)
Si1–O8	1.609(4)	1.607(3)	1.608(4)	1.606(4)	1.603(4)	1.604(4)	1.603(4)	1.600(4)	1.604(5)	1.602(5)	1.604(5)	1.613(4)
<Si1–O>	1.617	1.615	1.617	1.616	1.613	1.614	1.613	1.613	1.611	1.611	1.612	1.617
Volume	2.159	2.152	2.161	2.155	2.145	2.147	2.144	2.142	2.136	2.134	2.140	2.160
Si2–O2	1.630(4)	1.633(3)	1.629(4)	1.629(4)	1.629(4)	1.631(4)	1.623(4)	1.631(4)	1.640(5)	1.632(5)	1.620(5)	1.634(4)
Si2–O3	1.634(4)	1.628(4)	1.629(4)	1.632(4)	1.624(4)	1.626(4)	1.629(4)	1.632(4)	1.631(5)	1.633(5)	1.625(5)	1.634(4)
Si2–O6	1.600(3)	1.599(3)	1.597(4)	1.592(4)	1.591(4)	1.587(4)	1.590(4)	1.591(5)	1.574(6)	1.586(5)	1.585(4)	1.599(4)
Si2–O7	1.619(3)	1.620(3)	1.618(3)	1.616(4)	1.617(4)	1.617(4)	1.613(4)	1.615(5)	1.625(6)	1.617(5)	1.636(6)	1.625(4)
<Si2–O>	1.621	1.620	1.618	1.618	1.615	1.615	1.614	1.617	1.617	1.617	1.616	1.623
Volume	2.182	2.180	2.172	2.169	2.160	2.160	2.155	2.168	2.168	2.166	2.165	2.191
AlO₄ tetrahedra												
Al1–O4	1.757(4)	1.756(4)	1.758(4)	1.759(4)	1.755(4)	1.757(4)	1.762(5)	1.769(4)	1.754(5)	1.762(5)	1.768(5)	1.755(4)
Al1–O5	1.754(3)	1.751(3)	1.747(4)	1.749(4)	1.753(4)	1.751(4)	1.754(4)	1.746(5)	1.745(6)	1.750(5)	1.753(6)	1.750(4)
Al1–O6	1.718(3)	1.718(3)	1.718(4)	1.716(4)	1.720(4)	1.717(4)	1.716(4)	1.708(5)	1.721(6)	1.711(5)	1.711(6)	1.715(4)
Al1–O8	1.760(4)	1.756(3)	1.751(4)	1.759(4)	1.756(4)	1.756(4)	1.753(4)	1.760(4)	1.766(5)	1.758(5)	1.758(6)	1.756(4)
<Al1–O>	1.747	1.745	1.744	1.746	1.746	1.745	1.746	1.746	1.746	1.745	1.747	1.744
Volume	2.729	2.720	2.711	2.721	2.722	2.718	2.724	2.722	2.723	2.719	2.729	2.712
Al2–O1	1.744(3)	1.747(3)	1.743(4)	1.747(4)	1.742(4)	1.742(4)	1.743(4)	1.747(5)	1.752(7)	1.753(6)	1.750(6)	1.753(4)
Al2–O2	1.743(4)	1.734(3)	1.741(4)	1.737(4)	1.736(4)	1.736(4)	1.742(4)	1.733(4)	1.730(5)	1.732(5)	1.735(5)	1.736(4)
Al2–O3	1.754(4)	1.754(3)	1.750(4)	1.747(4)	1.756(4)	1.755(4)	1.751(4)	1.752(5)	1.755(6)	1.744(5)	1.755(6)	1.753(4)
Al2–O7	1.736(4)	1.738(3)	1.739(4)	1.737(4)	1.738(4)	1.740(4)	1.735(4)	1.740(4)	1.738(5)	1.742(5)	1.734(4)	1.744(4)
<Al2–O>	1.744	1.743	1.743	1.742	1.743	1.743	1.743	1.743	1.744	1.743	1.743	1.747
Volume	2.691	2.686	2.685	2.678	2.684	2.684	2.683	2.682	2.686	2.680	2.686	2.703
SrO₇ polyhedra												
Sr–O1	2.649(3)	2.657(3)	2.659(4)	2.661(4)	2.671(4)	2.677(4)	2.683(4)	2.687(4)	2.698(5)	2.701(5)	2.707(5)	2.653(4)
Sr–O2	2.674(4)	2.683(3)	2.685(4)	2.701(4)	2.706(4)	2.711(4)	2.726(4)	2.734(4)	2.729(6)	2.750(5)	2.771(5)	2.675(4)
Sr–O3	2.659(3)	2.665(3)	2.670(4)	2.674(4)	2.677(4)	2.681(4)	2.687(4)	2.689(4)	2.690(5)	2.700(5)	2.698(5)	2.656(4)
Sr–O4	2.609(3)	2.618(3)	2.616(4)	2.621(4)	2.628(4)	2.628(4)	2.631(4)	2.631(4)	2.645(5)	2.649(5)	2.641(5)	2.617(4)
Sr–O5	2.612(3)	2.614(3)	2.614(4)	2.617(4)	2.621(4)	2.626(4)	2.626(4)	2.633(4)	2.638(5)	2.637(4)	2.635(5)	2.612(4)
Sr–O7	2.583(3)	2.581(3)	2.584(3)	2.591(4)	2.592(4)	2.592(4)	2.589(4)	2.596(4)	2.603(4)	2.601(5)	2.605(4)	2.580(4)
Sr–O8	2.722(4)	2.732(3)	2.745(4)	2.748(4)	2.762(4)	2.770(4)	2.780(4)	2.788(5)	2.785(6)	2.810(5)	2.820(6)	2.726(4)
<Sr–O>	2.644	2.650	2.653	2.659	2.665	2.669	2.676	2.681	2.684	2.693	2.696	2.646
Volume	24.852	24.993	25.094	25.265	25.421	25.520	25.717	25.828	25.915	26.175	26.208	24.893

Table 4. Bond distances and polyhedral parameters in slawsonite $SrAl_2Si_2O_8$ at different temperatures in the P–1 space group.

Temperature, °C	27	100	200
Temperature Point	**T00**	**T01**	**T02**
SiO$_4$ tetrahedra			
Si1–O2	1.620(5)	1.621(5)	1.621(5)
Si1–O4	1.615(4)	1.618(4)	1.618(5)
Si1–O5	1.610(5)	1.605(5)	1.606(5)
Si1–O13	1.620(4)	1.619(5)	1.614(5)
<Si1–O>	1.616	1.616	1.615
Volume	2.156	2.155	2.152
Si2–O3	1.621(4)	1.618(5)	1.624(5)
Si2–O8	1.628(4)	1.620(5)	1.621(5)
Si2–O10	1.610(4)	1.610(4)	1.621(5)
Si2–O12	1.610(4)	1.612(5)	1.612(5)
<Si2–O>	1.617	1.615	1.619
Volume	2.160	2.151	2.169
Si3–O6	1.624(4)	1.624(5)	1.622(5)
Si3–O7	1.634(4)	1.637(5)	1.629(5)
Si3–O9	1.631(4)	1.623(5)	1.630(5)
Si3–O14	1.599(4)	1.600(5)	1.597(5)
<Si3–O>	1.622	1.621	1.620
Volume	2.188	2.182	2.180
Si4–O1	1.612(4)	1.612(5)	1.614(5)
Si4–O11	1.631(4)	1.630(5)	1.628(5)
Si4–O15	1.628(4)	1.635(5)	1.632(5)
Si4–O16	1.599(4)	1.597(5)	1.597(5)
<Si4–O>	1.618	1.618	1.618
Volume	2.170	2.173	2.170
AlO$_4$ tetrahedra			
Al1–O4	1.752(4)	1.748(5)	1.745(5)
Al1–O5	1.752(5)	1.758(5)	1.752(5)
Al1–O8	1.762(5)	1.762(5)	1.760(5)
Al1–O16	1.718(4)	1.716(5)	1.714(5)
<Al1–O>	1.746	1.746	1.742
Volume	2.723	2.723	2.707
Al2–O2	1.760(5)	1.757(5)	1.754(5)
Al2–O10	1.755(4)	1.752(5)	1.745(5)
Al2–O12	1.766(4)	1.758(5)	1.756(5)
Al2–O14	1.714(4)	1.716(5)	1.717(5)
<Al2–O>	1.749	1.746	1.743
Volume	2.736	2.722	2.707
Al3–O1	1.746(5)	1.744(5)	1.744(5)
Al3–O9	1.750(4)	1.754(5)	1.749(5)
Al3–O13	1.745(4)	1.745(5)	1.744(5)
Al3–O15	1.741(5)	1.734(5)	1.740(5)
<Al3–O>	1.746	1.744	1.744
Volume	2.696	2.690	2.691
Al4–O3	1.740(4)	1.744(5)	1.744(5)
Al4–O6	1.728(4)	1.735(5)	1.733(5)
Al4–O7	1.746(4)	1.736(5)	1.739(5)
Al4–O11	1.756(4)	1.753(5)	1.752(5)
<Al4–O>	1.743	1.742	1.742
Volume	2.684	2.679	2.679

Table 4. *Cont.*

Temperature, °C	27	100	200
Temperature Point	T00	T01	T02
SrO$_7$ polyhedra			
Sr1–O2	2.608(4)	2.612(4)	2.618(4)
Sr1–O5	2.724(4)	2.727(5)	2.742(5)
Sr1–O6	2.584(4)	2.580(4)	2.583(4)
Sr1–O9	2.660(4)	2.668(4)	2.670(4)
Sr1–O10	2.612(4)	2.616(4)	2.609(4)
Sr1–O13	2.648(4)	2.659(5)	2.664(5)
Sr1–O15	2.673(4)	2.682(4)	2.678(5)
<Sr1–O>	2.644	2.649	2.652
Volume	24.834	24.956	25.048
Sr2–O1	2.587(4)	2.586(4)	2.588(4)
Sr2–O3	2.653(4)	2.660(5)	2.655(5)
Sr2–O4	2.613(4)	2.612(4)	2.620(4)
Sr2–O7	2.671(4)	2.680(4)	2.686(5)
Sr2–O8	2.608(4)	2.621(4)	2.621(4)
Sr2–O11	2.666(4)	2.668(4)	2.675(4)
Sr2–O12	2.719(4)	2.731(5)	2.742(5)
<Sr2–O>	2.645	2.651	2.655
Volume	24.915	25.045	25.157

It is also worth noting, that 'Sr-feldspar' has not been yet discovered in nature. Strontium, having almost the same abundance in the Earth crust as barium (Sr 3.70×10^{-4}, Ba 4.25×10^{-4} mass fraction, kg/kg; [49]) have almost twice less valid mineral species containing it as an essential constituent (102 and 192, respectively; CNMNC IMA). Being smaller than Ba, strontium could substitute calcium in minerals much easier. As a result, it "dissolves" in other phases instead of having its own mineral species. Clay minerals (e.g., montmorillonite) are responsible for most of the exchange capacity for strontium in soils (e.g., [50]). Zeolites [51] and Mn (oxy)hydroxides also exchange or could sorb strontium [52,53].

3.2. Slawsonite Thermal Expansion

Thermal expansion coefficients (TECs) calculated both with the linear and second-order polynomial approximation of the unit-cell parameters are listed in Table 5. The following approximate equations for the unit cell parameters were obtained:

$a(T) = 8.329(2) + 0.000054(1)T + 0.000000027(9)T^2$ ($R^2 = 0.992$);
$b(T) = 9.362(2) + 0.000019(1)T + 0.000000007(9)T^2$ ($R^2 = 0.933$);
$c(T) = 8.893(2) + 0.000071(8)T + 0.000000024(8)T^2$ ($R^2 = 0.996$);
$\beta(T) = 90.25(2) + 0.00008(8)T + 0.000000001(7)T^2$ ($R^2 = 0.694$);
$V(T) = 693.4(3) + 0.011(1)T + 0.000005(1)T^2$ ($R^2 = 0.996$).

Regardless of the approximation method, the thermal expansion of slawsonite has quite an anisotropic character. The maximum and minimum expansion was observed along the *c* and *b* axes, correspondingly, i.e., in the plane of four- and eight-membered rings of TO_4 (*T* = Si, Al) tetrahedra (Figure 2). Such behavior could be explained by the hinge deformation mechanism, which was previously noted for isotypic danburite-group minerals [32].

The linear approximation of the unit cell parameters has also been done for the three separate parts according to their inflections (27–200, 300–700, and 800–1000 °C), but the R^2 fitting values for all parameters were not reasonable (below 0.9 and for some parameters below 0.5). So, all the data were used together for TECs calculation. It is worth noting that the β angle fitting was not precise enough both in whole and in the three separate data sets, which is associated with the general problems of the β determination.

Table 5. TECs ($\times 10^6$ °C^{-1}) of slawsonite along the principal axes of the thermal expansion tensor and crystallographic axes.

T, °C	α_{11}	α_{22}	α_{33}	μ ($\alpha_{33}\hat{\ }c$)	α_a	α_b	α_c	α_β	α_V
				Linear approximation					
27–1000	9.4(4)	2.9(3)	11.2(3)	28.0(2)	9.8(4)	2.9(3)	10.7(3)	0.9(2)	23.4(6)
				Quadratic polynomial approximation					
27	6(1)	2(1)	8.4(9)	22.0(9)	7(1)	2(1)	8.2(9)	0.9(8)	17(1)
300	8.1(6)	2.5(5)	9.9(4)	25.1(4)	8.4(6)	2.5(5)	9.6(4)	0.9(4)	20.6(9)
700	10.5(5)	3.1(5)	12.2(4)	31.3(4)	11.0(5)	3.1(5)	11.7(4)	0.9(4)	25.9(8)
1000	12(1)	4(1)	13.9(9)	37.1(8)	13(1)	4(1)	13.3(9)	0.9(8)	30(1)

The observed bond lengths and polyhedral volumes for slawsonite at different temperatures are given in Table 3. The expansion of the three types of polyhedral (SrO$_7$, SiO$_4$, and AlO$_4$) are significantly different, which is consistent with other studies of alumino- and borosilicate compounds (e.g., [19,31], etc.).

In the whole temperature range, Sr atoms are coordinated by seven oxygen atoms. As it was mentioned above, Sr atoms are located in the cavities of eight-membered rings of TO_4 (T = Si, Al) tetrahedra. If we consider the crystal structure of slawsonite as consisting of the layers of four- and eight-membered rings of TO_4 tetrahedra, Sr atoms are located between these layers (Figure 3b). Wherein O1, O4, O5, and O5 atoms belong to the layer consisting of Al1O$_4$ and Si1O$_4$ tetrahedra, whereas O2, O3, and O7 atoms belong to the layer of Al2O$_4$ and Si2O$_4$ tetrahedra. All Sr–O bonds increase continuously with the increasing temperature (Figure 6): three longest bonds (Sr–O2, Sr–O8 and Sr–O1), located parallel to the c axis, demonstrate the most intense increase (first two increase by 3.6%, whereas the last one by 2.2%). The elongation of four other bonds, located close to the b axis, is in the range of 0.5–1.5%. Such bond behavior agrees with the thermal expansion of the whole crystal structure, as the maximal and minimal thermal expansion is along the c and b axes, respectively (Table 5). Generally, in the whole studied temperature range, the volume of SrO$_7$ polyhedra increases up to 5.5%.
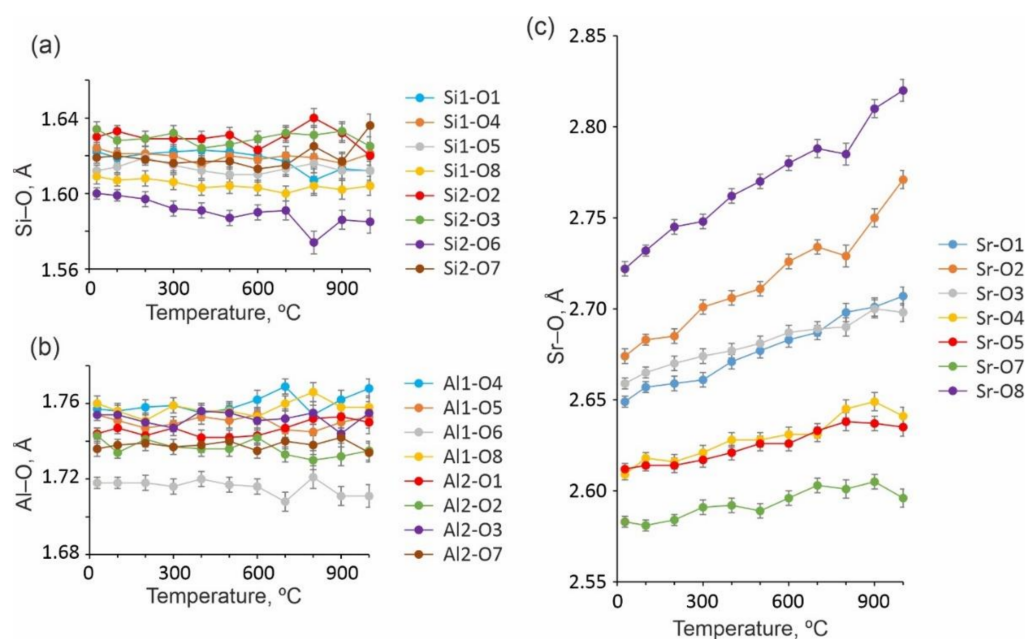
Figure 6. Temperature dependence of Si–O (**a**), Al–O (**b**), and Sr–O (**c**) interatomic distances in the crystal structure of slawsonite.

The changes in the bond-lengths of AlO$_4$ and SiO$_4$ tetrahedra are not so intense (Table 3, Figure 6a,b), i.e., do not exceed 0.02 Å or 0.3%. This fact agrees with the general

idea about the model of the rigid-unit mode [54–56] and the idea of cooperative motions of tetrahedral groups, such as titling and rotating [57]. It should also be noted that these changes are negative: only Si2–O7, Al1–O4, Al2–O1, and Al2–O3 bonds slightly increase, whereas all other bonds decrease.

4. Conclusions

Based on in situ high-temperature single-crystal X-ray diffraction data we can conclude, that $(Sr_{1-x}Ba_x)Al_2Si_2O_8$ (x < 0.03) could exist only in one polymorph modification (Sp. gr. $P2_1/c$) in a temperature up to 1000 °C despite non-linear behavior of the unit cell parameters. Natural compounds with stoichiometry close to slawsonite and high Ca/Ba content should be carefully checked by X-ray diffraction techniques. Our results compared with data of Tagai et al. [33] show that several polymorphs could potentially occur at the same deposit, but for their determination, single-crystal X-ray diffraction studies are necessary.

Generally, the thermal expansion of the unit-cell parameters of slawsonite is very close to that of danburite-group minerals $MB_2Si_2O_8$ (M = Ca, Sr, Ba) [32], i.e., the feldspar-related minerals with the paracelsian topology. For all four compounds the directions of maximal and minimal thermal expansion are located on the plane of four- and eight-membered rings, which is associated with the hinge deformations of eight-membered rings. Gorelova et al. [32] mentioned that the increase of the extra framework cation size (from Ca to Ba) leads to the increase of the thermal expansion anisotropy and volume thermal expansion. This study showed that not only the extra framework cation, but also the framework forming cation (the replacement of B (0.11 Å) to Al (0.39 Å) [45]) causes similar changes: under ambient conditions $\alpha_{max}/\alpha_{min}$ = 2 and 4 and α_V = 15 and 17 × 10^6 °C^{-1} for pekovite ($SrB_2Si_2O_8$) and slawsonite, respectively.

The comparison of the behavior of slawsonite under high-temperature (up to 1000 °C) and high-pressure (up to 6 GPa [29]) conditions (Figure 3) demonstrate the similarity of deformations in the layer of four- and eight-membered rings (i.e., in the *bc* plane) and differences in other directions. Generally, in both cases, the deformations are quite anisotropic, but under temperature increase, the minimal changes are along the *b* axis, whereas under pressure increase the structure remains almost unchanged along the *a*-axis, i.e., parallel to the extension of the crankshaft chains.

References

1. Chen, S.; Zhu, D.-G.; Cai, X.-S. Low-temperature densification sintering and properties of monoclinic-SrAl$_2$Si$_2$O$_8$ ceramics. *Metall. Mater. Trans. A* **2014**, *45*, 3995–4001. [CrossRef]
2. Chen, S.; Zhu, D.-G. Low-temperature sintering behavior and properties of monoclinic-SrAl$_2$Si$_2$O$_8$ ceramics prepared via an aqueous suspension milling process. *J. Mater. Sci. Mater. Electron.* **2016**, *27*, 11127–11136. [CrossRef]
3. Zhao, S.; Qin, S.; Jia, Z.; Fu, S.; He, P.; Duan, X.; Yang, Z.; Li, D.; Jia, D.; Zhang, J.; et al. From bulk to porous structures: Tailoring monoclinic SrAl$_2$Si$_2$O$_8$ ceramic by geopolymer precursor technique. *J. Am. Ceram. Soc.* **2020**, *130*, 4957–4968. [CrossRef]

4. Li, L.; Liu, X. Effects of changing the M^{2+} cation on the crystal structure and optical properties of divalent samarium-doped $MAl_2Si_2O_8$ (M = Ca, Sr, Ba). *RSC Adv.* **2015**, *5*, 19734. [CrossRef]

5. Li, X.; Yang, C.; Liu, Q.; Wang, X.; Mi, X. Enhancement of luminescence properties of $SrAl_2Si_2O_8$: Eu^{3+} red phosphor. *Ceram. Int.* **2020**, *46*, 17376–17382. [CrossRef]

6. Dai, W.; Hu, J.; Liu, G.; Xu, S.; Huang, K.; Zhou, J.; Xu, M. Thermometer of stable $SrAl_2Si_2O_8$: Ce^{3+}, Tb^{3+} based on synergistic luminescence. *J. Lumin.* **2020**, *217*, 116807. [CrossRef]

7. Wang, B.; Kong, Y.; Chen, Z.; Li, X.; Wang, S.; Zeng, Q. Thermal stability and photoluminescence of Mn^2 activated green-emitting feldspar phosphor $SrAl_2Si_2O_8$: Mn^2 for wide gamut w-LED backlight. *Opt. Mater.* **2020**, *99*, 109535. [CrossRef]

8. Xue, J.; Song, M.; Noh, H.M.; Park, S.H.; Choi, B.C.; Kim, J.H.; Jeong, J.H.; Du, P. Achieving non-contact optical thermometer via inherently Eu^{2+}/Eu^{3+}-activated $SrAl_2Si_2O_8$ phosphors prepared in air. *J. Alloys Compd.* **2020**, *843*, 155858. [CrossRef]

9. Yang, C.; Liu, Q.; Li, G.; Zhang, X.; Bai, Z.; Wang, X.; Mi, X. Tunable white light emission of rare earth ions doped single matrix $SrAl_2Si_2O_8$ phosphors. *J. Mater. Sci. Mater. Electron.* **2020**, *31*, 1057–1064. [CrossRef]

10. Ibarra, M.N.; Almanza, J.M.; Cortes, H.D.A.; Escobedo, B.J.C.; Martinez-Lopez, R. Chemical interaction between $SrAl_2Si_2O_8$ and molten aluminum. *J. Eur. Ceram. Soc.* **2015**, *35*, 4287–4292. [CrossRef]

11. Luo, J.; Li, X.; Zhang, F.; Chen, S.; Ren, D. Sintering of monoclinic $SrAl_2Si_2O_8$ ceramics and their Sr immobilization. *Int. J. Miner. Metall. Mater.* **2021**, *28*, 1057–1062. [CrossRef]

12. Papynov, E.K.; Belov, A.A.; Shichalin, O.O.; Buravlev, I.Y.; Azon, S.A.; Golub, A.V.; Gerasimenko, A.V.; Parotkina, Y.A.; Zavjalov, A.P.; Tananaev, I.G.; et al. $SrAl_2Si_2O_8$ ceramic matrices for ^{90}Sr immobilization obtained via spark plasma sintering-reactive synthesis. *Nucl. Eng. Technol.* **2021**, *53*, 2289–2294. [CrossRef]

13. Tang, H.; Shu, X.; Huang, W.; Miao, Y.; Shi, M.; Chen, S.; Li, B.; Luo, F.; Xie, Y.; Shao, D.; et al. Rapid solidification of Sr-contaminated soil by consecutive microwawe sintering: Mechanism and stability evaluation. *J. Hazard. Mater.* **2021**, *407*, 124761. [CrossRef] [PubMed]

14. Krivovichev, S.V. Feldspar polymorphism: Diversity, complexity, stability. *Zap. RMO Proc. Russ. Miner. Soc.* **2020**, *149*, 16–66.

15. Matysek, D.; Jirasek, J. Occurrences of slawsonite in rocks of the Teschenite association in the Podbeskydi piedmont area (Chech Republic) and their petrological significance. *Can. Mineral.* **2016**, *54*, 1129–1146. [CrossRef]

16. Griffen, D.T.; Ribbe, P.H.; Gibbs, G.V. The structure of slawsonite, a strontium analog of paracelsian. *Am. Mineral.* **1977**, *62*, 31–35.

17. Barrer, R.M.; Marshall, D.J. Hydrothermal chemistry of silicates. Part XII. Synthetic strontium aluminosilicates. *J. Chem. Soc.* **1964**, 485–497. [CrossRef]

18. Chiari, G.; Calleri, M.; Bruno, E.; Ribbe, P.H. The structure of partially disordered synthetic strontium feldspar. *Am. Mineral.* **1975**, *60*, 111–119.

19. Benna, P.; Bruno, E. Single-crystal in situ high-temperature structural investigation on strontium feldspar. *Am. Mineral.* **2001**, *86*, 690–696. [CrossRef]

20. Rocquefelte, X.; Clabau, F.; Paris, M.; Deniard, P.; Le Mercier, T.; Jobic, S.; Whangbo, M. Resolving the aluminium ordering in alumosilicates by a combined experimental / theoretical study of 27Al electric field gradients. *Inorg. Chem.* **2007**, *46*, 5456–5458. [CrossRef]

21. Nedic, B.; Kremenovic, A.; Dondur, V.; Dimitrijevic, R. Strontium deficient feldspar—Structure and X-ray powder diffraction line broadering analysis. *Cryst. Res. Technol.* **2008**, *43*, 266–272. [CrossRef]

22. Nedic, B.; Kremenovic, A.; Dimitrijevic, R.; Dondur, V. Crystal structures of Sr-diphylloalumosilicates synthesized from LTA and FAU zeolites. *Solid State Sci.* **2008**, *10*, 154–159. [CrossRef]

23. Al Saghir, K.; Chenu, S.; Veron, E.; Fayon, F.; Suchomel, M.; Genevois, C.; Porcher, F.; Matzen, G.; Massiot, D.; Allix, M. Transparency through structural disorder: A new concept for innovative transparent ceramics. *Chem. Mater.* **2015**, *27*, 508–514. [CrossRef]

24. Firror, R.L.; Seff, K. Near zero coordinate Ca^{2+} and Sr^{2+} in zeolite A. Crystal structures of dehydrated Ca6–A and Sr6–A. *J. Am. Chem. Soc.* **1978**, *100*, 3091–3096. [CrossRef]

25. Bahat, D. Homogeneous and heterogeneous polymorphic transformations in alkaline earth feldspars. *J. Mater. Sci.* **1978**, *13*, 2548–2554. [CrossRef]

26. Pakhomova, A.S.; Bykova, E.; Bykov, M.; Glazyrin, K.; Gasharova, B.; Liermann, H.-P.; Mezouar, M.; Gorelova, L.A.; Krivovichev, S.V.; Dubrovinsky, L. Closer look into close packing: Pentacoordinated silicon in the high-pressure polymorph of danburite. *IUCrJ* **2017**, *4*, 671–677. [CrossRef] [PubMed]

27. Gorelova, L.A.; Pakhomova, A.S.; Krivovichev, S.V.; Dubrovinsky, L.S.; Kasatkin, A.V. High pressure phase transitions of paracelsian $BaAl_2Si_2O_8$. *Sci. Rep.* **2019**, *9*, 12652. [CrossRef] [PubMed]

28. Gorelova, L.A.; Pakhomova, A.S.; Krzhizhanovskaya, M.G.; Winkler, B.; Krivovichev, S.V.; Dubrovinsky, L.S. Pressure-induced phase transitions in danburite-type borosilicates. *J. Phys. Chem. C* **2020**, *124*, 26048–26061. [CrossRef]

29. Gorelova, L.A.; Pakhomova, A.S.; Krzhizhanovskaya, M.G.; Pankin, D.V.; Krivovichev, S.V.; Dubrovinsky, L.S.; Kasatkin, A.V. Crystal structure evolution of slawsonite $SrAl_2Si_2O_8$ and paracelsian $BaAl_2Si_2O_8$ upon compression and decompression. *J. Phys. Chem. C* **2021**, *125*, 13014–13023. [CrossRef]

30. Pakhomova, A.; Aprilis, G.; Bykov, M.; Gorelova, L.; Krivovichev, S.; Belov, M.P.; Abrikosov, I.A.; Dubrovinsky, L. Penta- and hexa-coordinated beryllium and phosphorous in high-pressure modifications of $CaBe_2P_2O_8$. *Nat. Comm.* **2019**, *10*, 2800. [CrossRef]

31. Sugiyama, K.; Takeuchi, Y. Unusual thermal expansion of a B–O bond in the structure of danburite $CaB_2Si_2O_8$. *Z. Kristallogr.* **1985**, *173*, 293–304. [CrossRef]

32. Gorelova, L.A.; Filatov, S.K.; Krzhizhanovskaya, M.G.; Bubnova, R.S. High temperature behavior of danburite-like borosilicates $MB_2Si_2O_8$ (*M* = Ca, Sr, Ba). *Phys. Chem. Glasses-Eur. J. Glass Sci. Technol. B* **2015**, *56*, 189–196. [CrossRef]

33. Tagai, T.; Hoshi, T.; Suzuki, M.; Kato, A.; Matsubara, S. A new modification of slawsonite, $SrAl_2Si_2O_8$. *Z. Kristallogr.* **1995**, *210*, 741–745. [CrossRef]

34. Tasaryova, Z.; Fryda, J.; Janousek, V.; Racek, M. Slawsonite-celsian-hyalophane assemblage from a picrate sill (Prague Basin, Czech Republic). *Am. Mineral.* **2014**, *99*, 2272–2279. [CrossRef]

35. Bambauer, H.U.; Nager, H.E. Gitterkonstanten und displazive Transformation synthetischer Erdalkalifeldspaete. I. System $CaAl_2Si_2O_8$–$SrAl_2Si_2O_8$–$BaAl_2Si_2O_8$. *Neues Jahrb. Miner. Abh.* **1981**, *141*, 225–239.

36. McCauley, R.A. Polymorphism and dielectric electric properties of Ba- and Sr-containing feldspars. *J. Mater. Sci.* **2000**, *35*, 3939–3942. [CrossRef]

37. Toepel-Schadt, J.; Mueller, W.F.; Pentinghaus, H. Transmission electron microscopy of $SrAl_2Si_2O_8$: Feldspar and hexacelsian polymorphs. *J. Mater. Sci.* **1978**, *13*, 1809–1816. [CrossRef]

38. Bruno, E.; Gazzoni, G. Single-crystal X-ray investigations on strontium feldspar. *Z. Kristallogr.* **1970**, *132*, 327–331. [CrossRef]

39. Raman, C.V.; Nedungadi, T.M.K. The α–β transformation of quartz. *Nature* **1940**, *145*, 147. [CrossRef]

40. Agilent. *CrysAlis PRO*; Agilent Technologies: Oxfordshire, UK, 2012.

41. Sheldrick, G.M. A short history of SHELX. *Acta Crystallogr. A* **2008**, *64*, 112. [CrossRef]

42. Filatov, S.K. *Vysokotemperaturnaya Kristallokhimiya. Teoriya, Metody I Rezul'taty Issledovanii (High-Temperature Crystal Chemistry: Theory, Methods and Results of Investigations)*; Nedra: Leningrad, USSR, 1990; p. 289. (In Russian)

43. Bubnova, R.S.; Firsova, V.A.; Filatov, S.K. Software for determining the thermal expansion tensor and the graphic representation of its characteristic surface (Theta to Tensor-TTT). *Glass Phys. Chem.* **2013**, *39*, 347–350. [CrossRef]

44. Smith, J.V.; Brown, W.L. *Feldspar Minerals*; Springer: Berlin/Heidelberg, Germany, 1988; p. 828.

45. Shannon, R.D. Revised effective ionic radii and systematic studies of interatomic distances in halides and chalcogenides. *Acta Crystallogr. Sect. A Found. Adv.* **1976**, *32*, 751–767. [CrossRef]

46. Dimitrijević, R.; Dondur, V.; Kremenović, A. Thermally induced phase transformations of Ca-exchanged LTA and FAU zeolite frameworks: Rietveld refinement of the hexagonal $CaAl_2Si_2O_8$ diphyllosilicate structure. *Zeolites* **1996**, *16*, 294–300. [CrossRef]

47. Matsubara, S. The mineralogical implicartions of barium and strontium silicates. *Bull. Natl. Sci. Mus. Ser. C* **1985**, *11*, 37–95.

48. Nakajima, T.; Maruyama, S.; Matsuika, K. Metamorphism of the green rocks of the Ino Formation in central Shikoku. *J. Jpn. Assoc. Mineral. Petrol. Econ.* **1978**, *84*, 729–737. [CrossRef]

49. Lide, R.D. *CRC Handbook of Chemistry and Physics*; CRC Press LLC.: Boca Raton, FL, USA, 2004; p. 2712.

50. Goldsmith, W.A.; Bolch, W.E. Clay slurry sorption of carrier-free radiocations. *J. Sanit. Eng. Div. Proc. Am. Soc. Civ. Eng.* **1970**, *96*, 1115–1127. [CrossRef]

51. Ames, L.; Rai, D. Processes Influencing Radionuclide Mobility and Retention, Element Chemistry and Geochemistry, Conclusions and Evaluation. In *Radionuclide Interactions with Soil and Rock Media*; Pacific Northwest National Laboratory: Richland, WA, USA, 1978; Volume I, p. 327.

52. Siegel, M.; Bryan, C. Radioactivity, Geochemistry, and Health. In *Treatise on Geochemistry*, 2nd ed.; Holland, H.D., Turekian, K.K., Eds.; Elsiever: Amsterdam, The Netherlands, 2014; pp. 191–256.

53. Vereshchagin, O.S.; Perova, E.N.; Brusnitsyn, A.I.; Ershova, V.B.; Khudoley, A.K.; Shilovskikh, V.V.; Molchanova, E.V. Ferro-manganese nodules from the Kara Sea: Mineralogy, geochemistry and genesis. *Ore Geol. Rev.* **2019**, *106*, 192–204. [CrossRef]

54. Dove, M.T.; Cool, T.; Palmer, D.C.; Putnis, A.; Salje, H.; Winkler, B. On the role of Al–Si ordering in the cubic-tetragonal phase transition of leucite. *Am. Mineral.* **1993**, *78*, 486–492.

55. Dove, M.T.; Pride, A.K.A.; Keen, D.A. Phase transitions in tridimite studied using 'Rigid Unit Mode' theory, reverse Monte Carlo methods and molecular dynamics simulations. *Min. Mag.* **2000**, *64*, 267–283. [CrossRef]

56. Palmer, D.C.; Dove, M.T.; Ibberson, R.M.; Powell, B.M. Structural behavior, crystal chemistry, and phase transitions in substituted leucite: High resolution neutron powder diffraction studies. *Am. Mineral.* **1997**, *82*, 16–29. [CrossRef]

57. Hazen, R.M.; Finger, L.W. Polyhedral titling: A common type of pure displacive phase transition and its relationship to analcite at high pressure. *Phase Transit.* **1979**, *1*, 1–22. [CrossRef]